JOURNAL OF MATERIALS SCIENCE 27 (1992) 381–390

Fabrication and properties of SiC fibre-reinforced $Li_2O \cdot Al_2O_3 \cdot 6SiO_2$ glass–ceramic composites

JEN-YAN HSU, R. F. SPEYER
The New York State College of Ceramics, Alfred University, Alfred, NY 14802, USA

Ta_2O_5, Nb_2O_5 and TiO_2 were used separately as additives to a $Li_2O \cdot Al_2O_3 \cdot 6SiO_2$ glass–ceramic composition, to act as nucleating dopants and to aid the formation of an interfacial carbide layer (TaC and NbC) between the fibre and matrix in SiC fibre uniaxially reinforced glass–ceramic composites. The composites exhibited high modulus of rupture (>800 MPa) and fracture toughness ($K_{IC} > 15$ MPa $m^{1/2}$). The interfacial amorphous carbon rich layer and carbide layer were responsible for lowered interfacial shear strength but permitted high composite fracture toughness. The composite with the TiO_2 additive in the matrix showed a lower flexural strength (<500 MPa) and a smaller K_{IC} ($\simeq$11 MPa $m^{1/2}$) which resulted from the high interfacial shear strength between the SiC fibre and the matrix due to the formation of the interfacial TiC layer.

1. Introduction

Glass–ceramic matrix composite materials with fibres/whiskers as reinforcement have received much attention as high performance materials for elevated temperature applications [1–7]. These composites are expected to preserve the characteristics of their parent glass–ceramics, i.e. high elastic moduli and high melting points (or decomposition temperatures), and also demonstrate marked improvements in their fracture toughness, which approaches the values of some metals. The toughness increase of these composites is attributed to fibre debonding, fibre pull-out from the matrix [8–11], crack deflection, crack bridging, and crack impediment [6, 12–15].

Fibre reinforcement is considered superior to the use of whiskers (or short fibres and particulates) in optimizing the mechanical properties of composites. With long (or continuous) fibre reinforcement, fibre debonding and fibre pull-out are more prevalent and mechanical loading is transferred to the fibres which have much higher elastic moduli, and increases the mechanical strength of the composite [16, 17].

The optimum size of fibre reinforcements and their spacing within the brittle matrix composite, has been postulated as that needed in order to obtain an intact reinforcement effect on the matrix. The fibre spacing must therefore be smaller than the critical crack size which would lead to ultimate failure in the unreinforced material [12, 18]. The smaller fibre diameters are also desirable since their flexibility allows the fibres to be woven into various shapes for subsequent composite fabrication [19], and also to achieve the goal of minimizing the fibre spacing for a given packing geometry.

The development of fibre reinforced glass–ceramic matrix composites started in the early 1970s. Carbon/graphite fibres were utilized to reinforce glasses and glass ceramics, resulting in lightweight but strong and tough composites [20–24]. However, the severe oxidation of fibres at elevated temperatures in air has limited these materials as candidates for high temperature applications. Oxide fibres (Al_2O_3 [25, 26] and SiO_2[17]) were also applied as reinforcements in glass–ceramic matrix materials. But their mechanical properties are poor compared with the composites containing carbon/graphite fibres.

The invention of the fine polycrystalline β-SiC fibre (Nicalon*), sized 10–20 μm, from organometallic oxides [27] provided another excellent reinforcement material for composites in the high temperature application category, since in addition to its high mechanical strength and small available diameter, it promises to have a better resistance to high temperature oxidation [28–31]. In addition to the Nicalon SiC fibre yarn, several non-oxide and oxide fibre yarns, derived from organometallic precursors, have also been developed recently and applied as reinforcements in composites [19].

The Nicalon SiC fibre yarns have been used to reinforce glasses [32, 33], glass ceramics [16, 34], and more refractory ceramics [35, 36]. Among these, SiC fibre incorporated with lithia–alumina–silica glass ceramics has been a more successful composite [16, 17]. There are several advantages to the use of

*Ceramic Grade, Nippon Carbon Co., Ltd. Tokyo, Japan

0022–2461/92 $03.00 + .12

TABLE I Chemical compositions of glass batches for a composite matrix with various dopants of Ta_2O_5, Nb_2O_5, TiO_2 and ZrO_2

Glass	Wt %						
	Li_2O	Al_2O_3	SiO_2	Ta_2O_5	Nb_2O_5	TiO_2	ZrO_2
LAS I	5.29	18.06	63.87	12.78	0.00	0.00	0.00
LAS II	4.67	15.94	56.36	23.03	0.00	0.00	0.00
LAS III	5.14	17.55	62.06	0.00	15.25	0.00	0.00
LAS IV	5.42	18.53	65.54	0.00	5.00	3.64	1.87

glass or glass ceramics as matrix in fibre reinforced composites; (1) the composite can be easily densified without fibre damage because of the viscous flow of the glass matrix at composite densification temperatures, (2) heat treatment causes the glass matrix to devitrify and transform to a more refractory ceramic matrix, (3) high elastic modulus SiC fibres provide significant reinforcement to low modulus glasses or glass ceramics, (4) various chemical compositions and thus thermal expansion behaviour would provide a wide range of fibre–matrix interfacial stress options for the composite, (5) the stability of physical and chemical properties at elevated temperature is generally better than those of organic and metallic matrix materials, and (6) low density (2.2–2.7 gm cm^{-3}) [16, 17].

The toughness of fibre-reinforced composites, arising from energy absorption via fibre-pullout after matrix cracking, depends on the degree of coherence between the fibre and the matrix. If the fibre is either too strongly chemically bonded to the matrix, or too strongly held by radial compressive stresses imparted by the matrix, an increase in strength through modulus enhancement will occur but the composite will fail abruptly with cracking of the matrix. This is caused by fibres breaking in the plane of the advancing crack, without the composite exhibiting the fibre-pullout toughening effect. If there is neither chemical bonding nor frictional restraint between the fibre and the matrix, there will be no load sharing and therefore no property enhancement. Hence, obtaining an interfacial layer with optimum coherence between fibres and matrix is the most important condition of composite fabrication.

The Nicalon SiC fibre reinforced lithia aluminosilicate glass–ceramic matrix composite has proven to be a good competitor in this category. Its flexural strength has been reported as above 800 MPa and its fracture toughness (K_{IC}) about 17 MPa $m^{1/2}$ [5, 16]. Microstructure and microchemistry investigations by transmission electron microscopy (TEM), energy dispersive spectrometry (EDS), electron energy loss spectrometry (EELS) and scanning Auger electron spectrometry, revealed that an interfacial amorphous carbon rich layer between SiC fibre and matrix formed, and was responsible for the observed increase of toughness via fibre debonding and fibre pull-out from the matrix [37–39]. However, several later investigations indicated that with Nb_2O_5 additives in the raw materials of the matrix, an NbC layer formed between the aforementioned carbon layer and matrix. The formation of this NbC layer avoided the bubble-like pores which formed in the interfacial region and was believed due to the oxidation of SiC fibres (or foaming reaction between matrix and fibre) and resulted in the gas bubble formation [16, 40]. These pores caused the depletion of mechanical properties of the composite at room, as well as, high temperatures. Hence, the mechanical properties of these composites with the carbide interfacial layer are more promising [5, 8, 41].

In our early work [42, 43], Nb_2O_5 and Ta_2O_5 were proved to be effective nucleating agents in the $Li_2O \cdot Al_2O_3 \cdot 6SiO_2$ glass system. The crystallization mechanisms as well as devitrification processes of these glasses containing Nb_2O_5 or Ta_2O_5 were also characterized. The focus of this work was to incorporate the Nicalon SiC fibres in the aforementioned glass ceramics with these additives to fabricate a stronger and tougher composite. Nb and Ta are in the same group in the periodic table, and hence, Ta_2O_5 and Nb_2O_5 should have analogous chemical properties. Ta_2O_5 is thus expected to form an interfacial carbide layer. In this study, three sets of nucleating agents and additives for interfacial layer formation, Nb_2O_5, Ta_2O_5 and $TiO_2 \cdot ZrO_2/Nb_2O_5$, were added to the raw materials of glass batches of the composite matrix, respectively. In the first two additives, the dopant acted as a nucleating catalyst for the glass matrix, and as an agent for forming an interfacial carbide layer. The third set of additives include the well-known nucleating agents TiO_2 and ZrO_2, while Nb_2O_5 addition was used for the formation of the previously mentioned carbide layer. The objective of this investigation was to compare the effects of different dopants on the devitrification of glass matrices, the formation of an interfacial layer and ultimately, the mechanical properties of the composite.

2. Experimental procedure

2.1. Preparation of matrix material

The fabrication process of the glasses containing nucleating agents and additives for the composite matrix is identical to that in our previous work [42, 43]. Four glasses were prepared with chemical compositions as shown in Table I. Dopant additions for these glasses were: LAS I with 2.0 mol % Ta_2O_5, LAS II with 4.0 mol % Ta_2O_5, LAS III containing 4.0 mol % Nb_2O_5 and LAS IV with 3.0 mol % TiO_2, 1.0 mol % ZrO_2 and 1.88 mol % ($\approx$ 5.0 wt %) Nb_2O_5. These as-quenched glasses were crushed and ground to powders by a motor-driven mortar and pestle. The glass powders were then screened and granules smaller than 40 μm were ready for further size reduction by ball

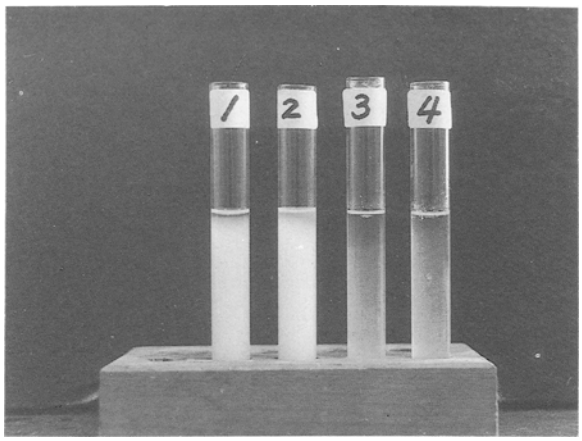

Figure 1 Sedimentation of glass powders in the slurries with addition of Trition X-405 in tube 1, Trition X-100 in tube 2, Darvan C in tube 3, and Darvan 821A in tube 4. The slurries were stirred at the same time and permitted to settle for 2 h before the picture was taken.

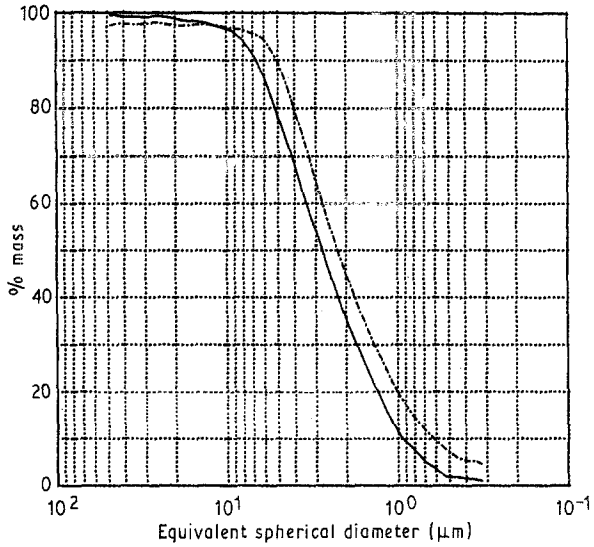

Figure 2 Particle size distribution of glass powders (LAS I) after 24 and 48 h (——) (– – –) ball milling, respectively.

milling. The larger particles were put back into the mortar and ground again.

Four different kinds of organic compounds, Trition X-100*, Trition X-405‡, Darvan C§, and Darvan 821A¶, were used as deflocculant to disperse the glass powders in a slurry for ball milling as well as for fibre infiltration (discussed later). Fig. 1 shows the deflocculation ability of these four compounds in suspensions containing these glass powders. The glass particles in solutions 3 and 4 rapidly agglomerated and sedimentated on the tube bottom, indicating that Darvan C and Darvan 821 were not effective deflocculants for these glass powders. Glass particles in the well-dispersed suspension containing Trition X-405 (tube 1) or Trition X-100 (tube 2) settled relatively slowly. Trition X-100, which had a deflocculation ability slightly better than that of Trition X-405, was chosen as the deflocculant in this study.

Partially stabilized zirconia beads were utilized as grinding media in the ball mill. The particle size distributions* of glass powders after 24 h and 48 h wet ball milling, respectively, are illustrated in Fig. 2. The average particle size was 3.6 μm (24 h) and 2.5 μm (48 h), respectively. In order to minimize contamination from the grinding media into the glass powders, ball milling for 24 h reduced the average particle size of glass powders to about 3 to 5 times smaller than the diameter of the Nicalon SiC fibre and was adequate for the hot pressing process to densify the glass matrices around the fibres.

2.2. Fabrication of composites

A slurry infiltration process (Fig. 3) was used to prepare the SiC fibre/glass powder tapes for further hot pressing. The continuous Nicalon SiC yarns, detached from a spool, were burned by a gas flame to remove a protective coating on the fibres provided by the manufacturer. The yarns were impregnated with an aqueous slurry containing the glass powders, and then collected on a rotating hexagonal drum which was covered

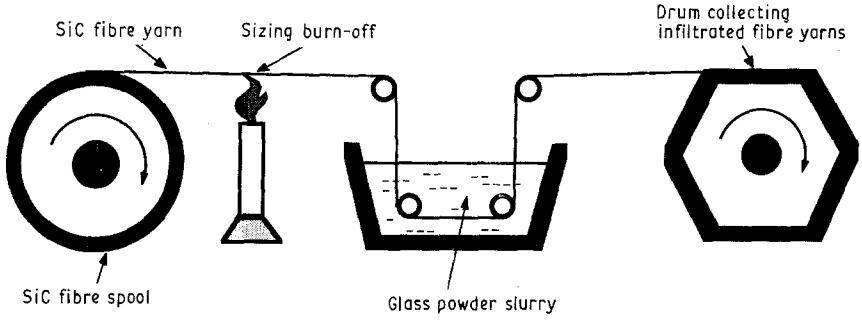

Figure 3 Slurry infiltration process.

* Emulsifier, wetting agent and detergent, Rohm & Haas Co., Philadelphia, PA
‡ Rohm & Haas Co.
§ Darvan C, R. T. Vanderbilt Company, Inc., Norwalk, CT
¶ Darvan 821A, R. T. Vanderbilt Company, Inc.
* Microscan particle size analyzer, Quantachrom Corp., Syosset, NY

TABLE II Organic compounds of the aqueous slurry systems for the slurry infiltration process

Slurry	Solids	Solvent	Binder	Plasticizer	Deflocculant	Defoamer
A	Glass powders	Water	Polyvinyl alcohol	Polyethylene glycol	Trition X-100	Napco NXZ
B	Glass powders	Water	Latex	Santicizer	Trition X-100	Napco NXZ

by Teflon cloth to prevent the wound fibre/powder slurry tape from sticking to the drum.

Two sets of organic compounds were used to prepare the slurry for the SiC yarn impregnation. Both systems were aqueous solutions and their constituents are illustrated in Table II. The slurry was prepared by mixing glass powders, water, deflocculant, binder, and plasticizer using a ball mill for another 24 h. The slurry viscosity was then measured by a Brookfield viscometer*. Slurry B, which was composed of Latex‡, Santicizer§, Trition X-100, glass powders, water and Napco NXZ¶ (defoamer), exhibited a relatively low viscosity of less than 2.0 poise. This viscosity was too low for these slurries to adhere to the SiC fibre yarn, and most of the slip dripped from the impregnated tapes before being dried. The viscosity of slurry A, containing polyvinyl alcohol◇ and polyethylene glycol□ was more applicable for slurry infiltration. Its viscosity varied from 3.0 to 20.0 poise, which increased as more solid and binder were added to the slurry. The viscosity of the slurry was used to control the relative volume percentage of fibre and matrix in the final composite.

The tapes were dried, cut, removed from the collecting drum, and then cut into 6 cm × 6 cm squares. The square tapes were then piled up with a unidirectional fibre alignment and put into a furnace for binder burn-out before being placed into a graphite die for hot pressing. Thermal gravimetric analysis△ (TGA) results of a typical dried tape (Fig. 4) shows that the weight loss due to burn-out of organic compounds occurred below 600 °C. Organic compounds in the slurry were therefore removed by thermal processing at 600 °C for 30 min.

The inside wall of the graphite die and pad blocks for hot pressing were coated with BN powder○ to avoid reaction with tapes during hot pressing and allowed the composites to be removed easily from the die after pressing. Hot pressing of composites was executed under a reducing atmosphere in an induction heated furnace. The typical hot pressing schedule of temperature and applied pressure is illustrated in Fig. 5. Pressure was applied to the stacked tapes in the graphite die in all cases at 1000 °C in order to avoid damaging the SiC fibres by unyielding granules. This

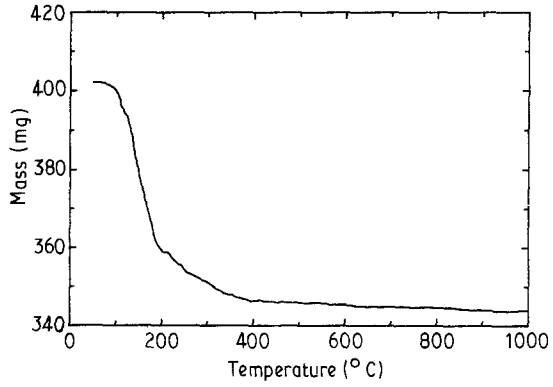

Figure 4 TGA curve for binder burn-out of tapes containing glass powder slurries.

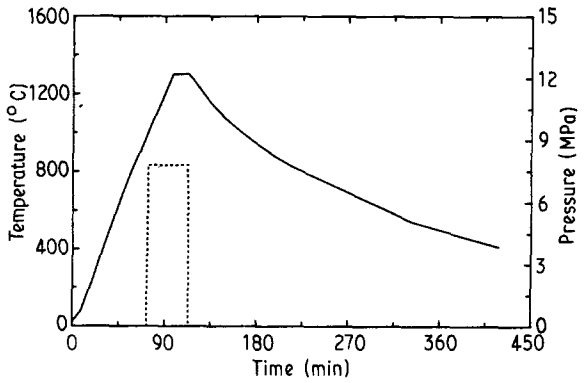

Figure 5 Hot pressing schedule for composite densification (—— temperature; ---- pressure).

temperature was about 150°–200 °C higher than the dilatometric softening point of the matrix glasses [43]. The soaking temperature was varied from 1200 °C–1400 °C and the holding time ranged from 0–30 min.

2.3. Characterization of composites

An optical microscope† was used to study the microstructure of the as-pressed composites in sections perpendicular and parallel to the alignment of the fibre. These sections were cut, ground, and then polished using diamond paste to 1 μm. The volume percentage

* LV Spindle #2, Brookfield Engineering Laboratories, Inc., Stoughton, MA
‡ Latex A1-608, Polysar Ltd., Sarnia, Candan
§ Santicizer 160, Monsanto Co., St. Louis, MO
¶ Henkel Process Chemical, Morriston, NJ
◇ Elvanol, Grade 72-60, E.I. du Pont Nemours & Co. Inc., Wilmington, DE
□ Carbowax 200, Union Carbide Corp., Danbury, CT
△ Harrop Industries, Inc., Columbus, OH, and Innovative Thermal System, Almond, NY
○ Boron Carbide, High Purity Powder, Union Carbide Co., Cleveland, OH
† Versamet-2, Unitron Instruments, Inc., Plainview, NY

of fibre and matrix in the composite was determined by using a scanning electron microscope* (SEM) with an image analysis‡ attachment. The area percentage of fibre and matrix on the polished section measured by the image analyzer is indicative of the volume percentage of both constituents in the composite since this distribution is expected to be consistent throughout the depth of the composite along the fibre axis direction. The microstructure and microchemistry of the interface regions between fibres and matrix were studied with a transmission electron microscope§ (TEM) with an accelerating voltage of 200 kV and an affixed energy dispersive spectrometer¶ (EDS). The results of these interfacial studies will be discussed in accompanying work [44]. The crystalline phases of the as-pressed composite samples which were ground and polished were characterized by a computer* interfaced X-ray (CuK_α) powder diffractometer‡ using a 2 s time constant and a step size of 0.02 degrees.

The composites were cut into approximately 55.0 × 1.8 × 2.2 mm bars with the longest specimen dimension parallel to the fibre axis for flexural strength tests. The strength of each sample set was determined from 20 bars of specimens from two different runs but with identical processing conditions to ensure reproducibility. The flexural test was performed under three-point-bending on an universal testing instrument§. The span was 45 mm between the two steel supporting beams of 3 mm in diameter. The cross-head speed rate for this test was 0.5 mm min^{-1}. The fracture toughness [45, 46] (K_{IC}) of these samples in the direction normal to the fibre alignment was measured under the identical sample preparation and testing conditions as those for the flexural strength test except that the testing bars were pre-notched using a diamond saw (0.3 mm in thickness) at a notched crack length/depth ratio of approximately 0.5. Each set of K_{IC} data was determined from five different tests. The equation [46]

$$K_{IC} = \frac{PS}{BW^{3/2}}\left[2.9\left(\frac{a}{W}\right)^{1/2} - 4.6\left(\frac{a}{W}\right)^{3/2} + 21.8\left(\frac{a}{W}\right)^{5/2} - 37.6\left(\frac{a}{W}\right)^{7/2} + 38.7\left(\frac{a}{W}\right)^{2/9}\right] \quad (1)$$

was used to calculate the K_{IC} value of composites, where P is the load, B is the width of specimen, S is the span length, W is the depth of sample and a is the crack length.

The interfacial shear strength between the matrix and an individual fibre was evaluated by a microhardness indenter¶. This analysis technique has been reported by several previous investigations [47–49].

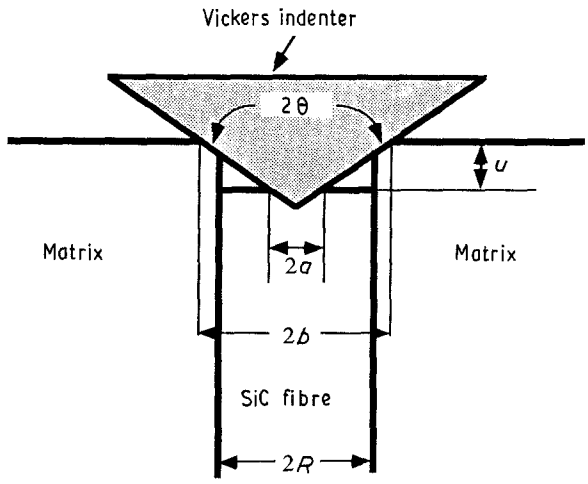

Figure 6 Schematic diagram of microhardness indentation method for measuring interfacial shear strength between the fibre and matrix.

A Vickers microhardness indenter was utilized, loaded onto the centre of each individual fibre on a polished section perpendicular to the fibre axis. The indentation load was 50 or 100 g with a 5 s hold. The diameter of the measured fibre ($2R$), the width of the indentation impression (in diagonal) on the fibre ($2a$) and on the matrix ($2b$) were measured and used to calculate the depressed displacement (u) of the fibre from the sample surface by the equation

$$u = (b - a)\cot\theta \quad (2)$$

where 2θ is the angle of Vickers indenter and is equal to 148°. The geometric relation for this equation is shown in Fig. 6. The interfacial shear strength (τ) can be evaluated by the equation [48]

$$\tau = \frac{a^4 H^2}{\pi^2 u R^3 E_f}$$

where H is the hardness of the SiC fibre measured on the fibres in the sections parallel to the fibre axis and E_f is the elastic modulus (200 GPa) [48]. Fifteen measurements were performed on each sample.

3. Results and discussion

3.1. Densification of composite and crystallization of matrix

Three slurries containing the same glass powders (LAS II in Table I) but with varying viscosity were used as matrices to fabricate composites which were all hot pressed to 1250 °C (pressure applied at 1000 °C), without holding, under an applied pressure of 6.9 MPa. The resulting composites are shown in Fig. 7. Many pores still remained in these composites

* Models 511-52, Autoscan, ETEC Co., Hayward, CA
‡ Models TS16-J018, Princeton Gamma Technology, Princeton, NJ 08504
§ Models FX2000, JOEL Ltd., Tokyo, Japan
¶ Models TS16-J018, Princeton Gamma Technology
* Models VAX-11/730, Digital Equipment Co., Northboro, MA
‡ Models 12045 X-ray diffraction unit, Phillips Electronic Instruments Co., Mount Vernon, NY
§ Models 1123, Universal Testing Instrument, Instron Co., Canton, MA
' Models HMV-2000, Shimadzu Microhardness Tester, Shimadzu Co., Kyoto, Japan

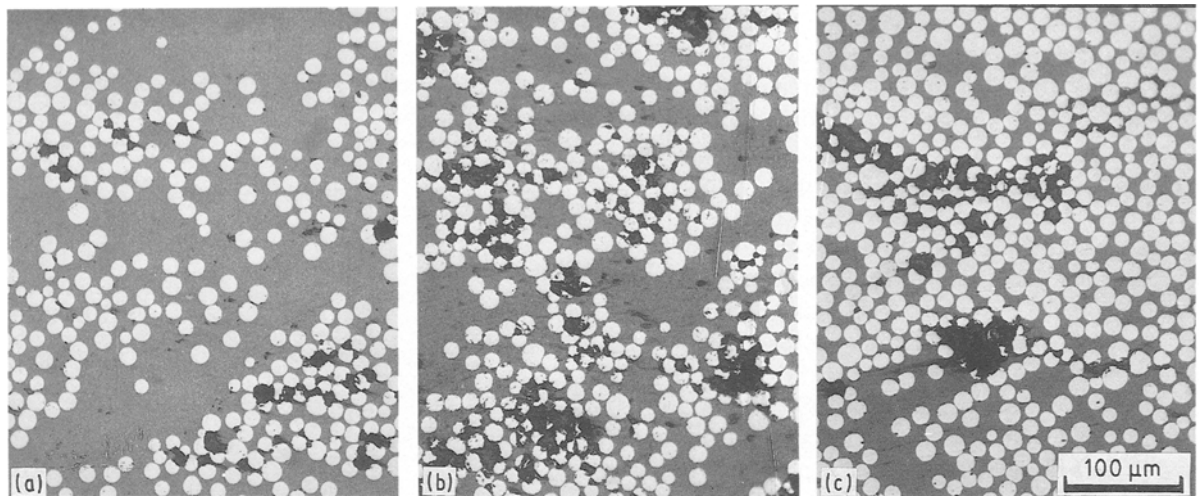

Figure 7 Microstructures of LAS II composites using three slurries with different viscosities: (a) 18 poise, (b) 13 poise, and (c) 9 poise. Large pores are observed in all three samples.

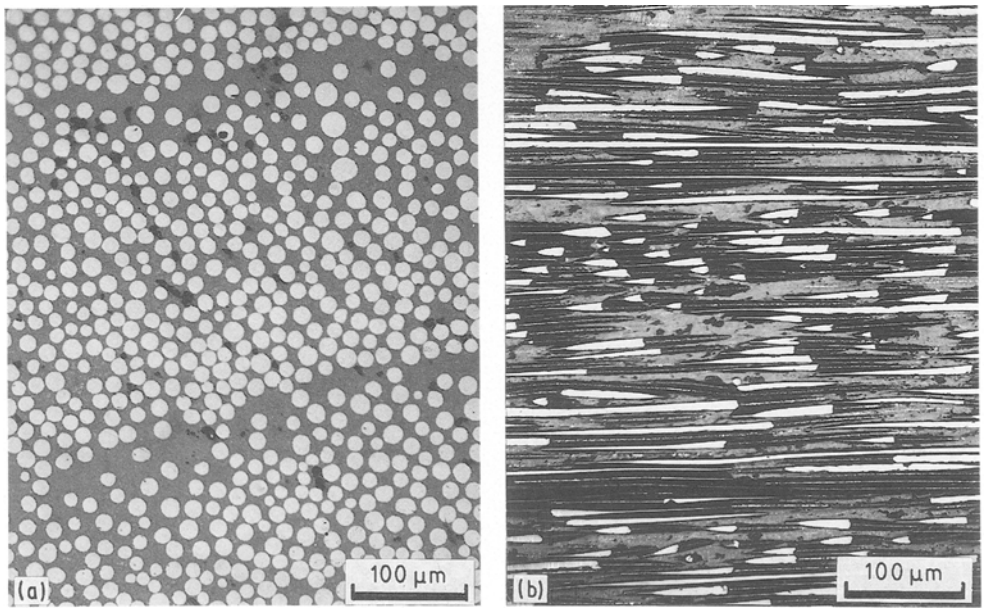

Figure 8 Microstructures of the more fully densified LAS II composite, sectioned (a) normal to the fibre axis and (b) parallel to the fibre axis. The vol % of SiC fibre in the composite was about 40%.

which indicated that hot pressing with these conditions (temperature and pressure) was inadequate to densify the composites. The micrographs also reveal that, as expected, less viscous slurries used in fabrication led to a higher volume content of SiC fibre in the final product (Fig. 7c).

Fig. 8a and b show a nearly fully densified microstructure of the LAS II composite with a bulk density (by Archimedean method) of $\approx 2.6\ \mathrm{gm\,cm^{-3}}$. This sample was hot pressed to 1300 °C and held for 15 min under a load pressure of 7.9 MPa (Fig. 5). The volume content of fibre in this sample was approximately 40%, as determined by SEM image analysis. The hot pressing conditions for generating densified composites utilizing different glass powders as matrix are given in Table III. A slightly higher temperature of 1400 °C was necessary to densify the LAS III composite under 7.9 MPa pressure.

From previous work [42, 43] using differential thermal analysis (DTA), devitrification occurred below the temperature at which pressure was applied (1000 °C) for all glass compositions. Although the glass powders were devitrified, application of pressure from 1000 °C to soaking temperatures (1300 °C–1400 °C) followed by a hold, acted to densify the matrix, undoubtably assisted by the viscous flow of residual glassy phase.

Fig. 9 shows the crystalline phases formed in the matrices of these as-pressed composites. β-spodumene SS was the major crystalline phase in all four matrices. Ta_2O_5 and TaC were the other two crystalline phases detected in the composite with the glass ceramic matrix containing Ta_2O_5 as a dopant. Nb_2O_5 and NbC were also observed in the composite with LAS III glass matrix (Nb_2O_5 additives). In the composite sample using LAS IV glass (containing TiO_2, ZrO_2 and Nb_2O_5 dopants) as the matrix, TiC, NbC and

TABLE III Hot pressing conditions for the densification of composites with various matrix materials

Matrix composition	Additives (mol %)	Temperature (°C)	Pressure (MPa)	Soaking time (min)
LAS I	Ta_2O_5/2.0	1350	7.9	15.0
LAS II	Ta_2O_5/4.0	1300/1350	7.9	15.0
LAS III	Nb_2O_5/4.0	1400	7.9	15.0
LAS IV	TiO_2/3.0, ZrO_2/1.0, Nb_2O_5/1.88	1350	7.9	15.0

TABLE IV Modulus of rupture and toughness, K_{IC}, (with standard deviation) of densified composites

Matrix composition	Hot pressing temperature (°C)	Modulus of rupture (MPa)	Toughness, K_{IC} (MPa $m^{1/2}$)
LAS I	1350	630.7 ± 29.9	15.6 ± 2.7
LAS II	1300	860.3 ± 76.3	17.0 ± 4.3
LAS II	1350	839.8 ± 42.9	15.7 ± 2.1
LAS III	1400	718.6 ± 61.7	14.1 ± 3.4
LAS IV	1350	445.0 ± 27.2	10.7 ± 2.8

ZrO_2 crystalline phases were also detected. In addition to the previous crystalline phases, the broadened (1 1 1) peak (most intense peak) of β–SiC, from 33° to 38° in 2θ, was also observed in the XRD spectra of these four composites. This was also confirmed by TEM (SAD) microstructural investigation of these samples in parallel work [44], which confirmed the fine polycrystalline structure of the SiC fibres. The appearances of TaC and NbC in these composites were in the interfacial regions between the SiC fibres and matrices [44].

3.2. Mechanical properties of composites

The average modulus of rupture of as-pressed composites are illustrated in Table IV. Two sets of as-pressed composites with 4.0 mol % Ta_2O_5 additives but different soaking temperatures (1300 °C and 1350 °C) exhibited high flexural strength (860 MPa and 840 MPa, respectively). The composites with LAS I and LAS III glass matrix failed at flexural stresses of ≈630 MPa and ≈720 MPa, respectively. The strength of these composites were about 3–4 times that of monolithic glass ceramics [50]. A typical stress versus crosshead displacement curve for LAS II composites using a three-point-bending test is shown in Fig. 10. Stress increased linearly with displacement to about 600 MPa, after which the behaviour was non-linear, reaching a maximum point at 1020 MPa, and then dropped at a rate slower than the catastrophic failure commonly associated with monolithic ceramics. LAS I and III composites had a similar behaviour. Fig. 11a shows that these composites failed on the compression side of specimens rather than on the

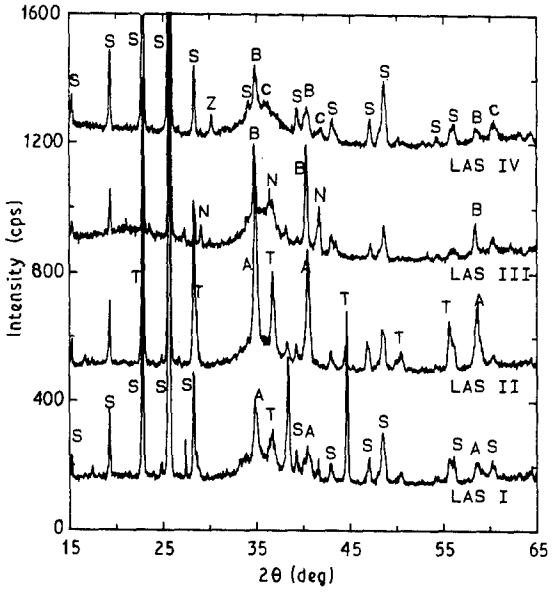

Figure 9 X-ray diffraction patterns of the as-pressed composites using various matrix materials. S is the β-spodumene SS phase; A = TaC; T = Ta_2O_5; B = NbC; N = Nb_2O_5; C = TiC and Z = ZrO_2 phase.

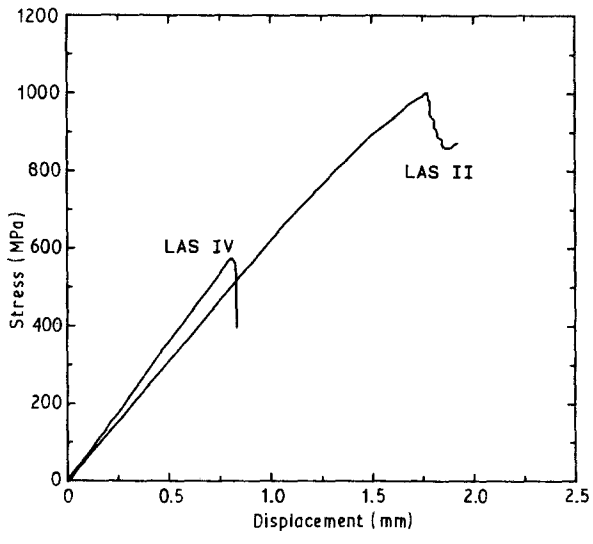

Figure 10 Typical stress versus displacement plot of LAS II and LAS IV composites.

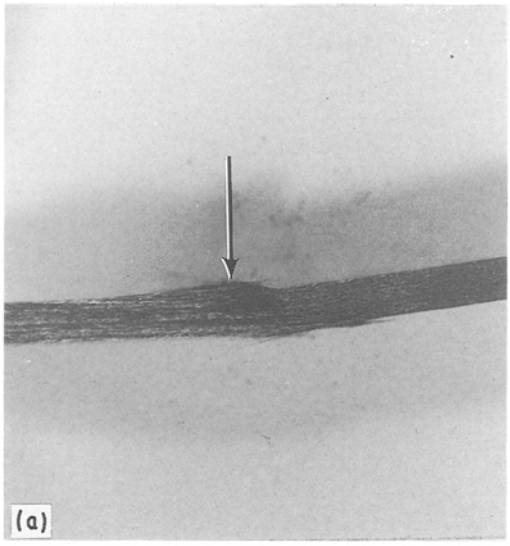

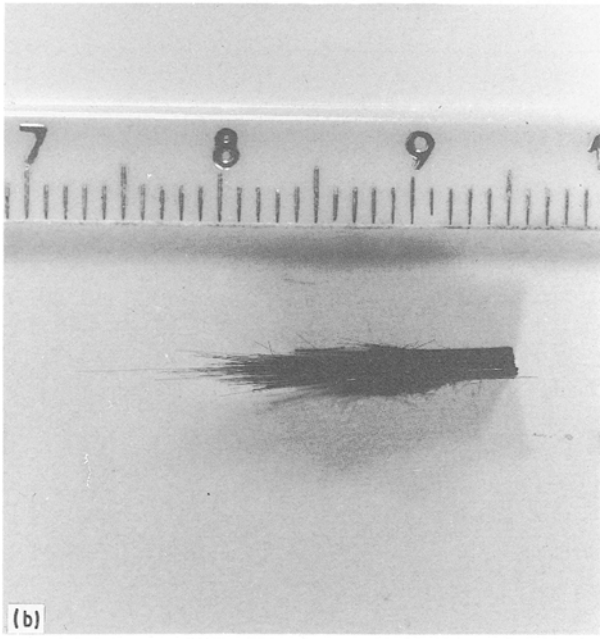

Figure 11 (a) Failure of the composite on the compression side (indicated by the arrow) of the composite specimen during bending test. (b) Fibre pull-out of the composite under tensile stress. Scale shown is 3 cm.

tension side during the bending test. This was also observed in other work [48]. It was interpreted that this phenomenon was due to low interfacial shear strength between fibre and matrix and hence delamination of the composite during the bending test, permitting the compression side of the sample under load to pop out. Fig. 11b illustrates the fibre pull-out failure of a sample under uniaxial tension in the fibre axis direction.

The composite with LAS IV glass as matrix demonstrated a smaller flexural strength of $\approx$450 MPa (Table IV). Its failure mechanism was quite different from that of LAS I, II and III composites. The failure of this composite occurred on the tensile surface of the specimen during the bending test (Fig. 12). Non-linear behaviour was not observed in the stress versus strain plot, and failure after the maximum strength was more like that of the catastrophic style of monolithic ceramics (Fig. 10).

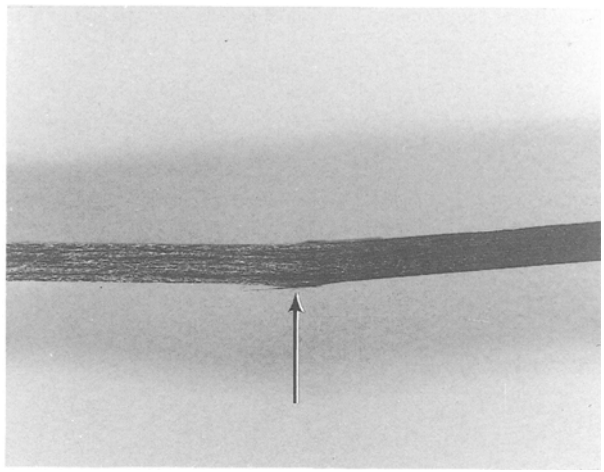

Figure 12 Tension side failure (shown by the arrow) of LAS IV composite during flexural strength test.

The values of critical stress intensity factor (K_{IC}) of these as-pressed composites are enumerated in Table IV. The K_{IC} value of the samples were above 14 MPa $m^{1/2}$, with exception of the composite with LAS IV as matrix (10.7 MPa $m^{1/2}$). Fig. 13 shows that during testing of these composites, instead of propagating forward, the pre-notched crack was blunted by a delamination parallel to the tape pile plane. These K_{IC} values are close to the reported data of similar composites from other publications [5, 16].

The interfacial shear strength, τ, (the strength needed to debond chemical cohesion and overcome frictional forces [10, 48]) between individual fibres and the matrix of the composite was calculated from the measured indenter impression and hardness data by the Vickers indentation method (Figs 6 and 14). The results are plotted in Fig. 15. The data spread was large (as was observed in early literature [49]), especially for the composites using LAS III and LAS IV

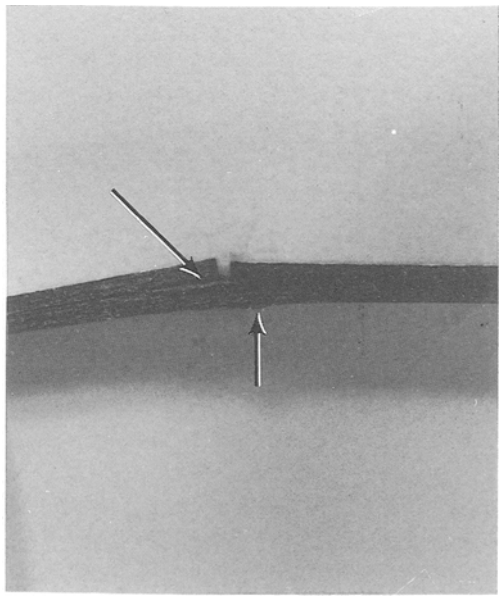

Figure 13 Delamination (shown by the longer arrow) of the composite blunted by the propagation of a pre-notched crack in the LAS III composite during the toughness test. The sample failed on the compression side (indicated by the short arrow).

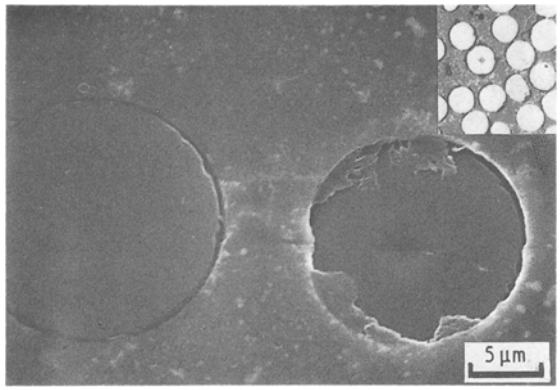

Figure 14 Indented fibre shows the impression of the indenter on the fibre and matrix (inset micrograph). The fibre was pushed down below the specimen surface (right) as compared with the unindented fibre (left).

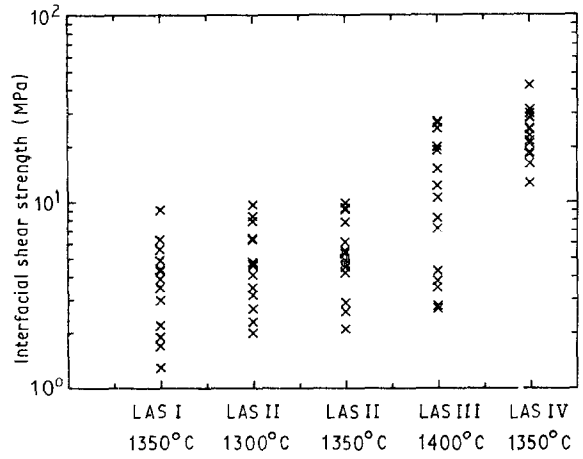

Figure 15 The distribution of interfacial shear strength (τ) for the LAS composites with different matrix compositions.

glasses as the matrix. This scatter was attributed to the fact that the uncertainty of indentation impression size would cause a possible two fold uncertainty in the calculated τ values. The uncertainty of impression size may be due to experimental error from the measurement of indentation impression on the fibre and matrix. Furthermore, local variation in stress distribution around each measured fibre due to varying fibre distribution densities would cause a spectrum of measured interfacial shear strength.

Composites composed of LAS I or LAS II glasses had small interfacial shear strengths, yielding average values of 4.0, 4.8 and 5.6 MPa (Fig. 15), respectively. However, the composites with the other two glass ceramics as the matrix had rather larger τ values: 12.5 (LAS III) and 23.0 (LAS IV) MPa. The higher densification temperature (1400 °C) apparently caused an increase in interfacial shear strength in the LAS III composite. The τ value of the LAS IV composite was nearly 4–5 times larger than that of the composites with LAS I or LAS II glass as well as values from other investigations [47, 49].

The smaller interfacial shear strength between the fibre and matrix in LAS I, LAS II and LAS III composites has led to a higher fracture toughness of the composites, as well as a larger modulus of rupture (Table IV). The amorphous carbon rich layer and the carbide layer (NbC and TaC) [44], observed in Fig. 9, in the interfacial region, are responsible for the lower interfacial shear strength (τ). The larger τ value of LAS IV composite (Fig. 16) was responsible for the lower measured toughness in that composite. This is believed to be due to the addition TiO_2 to the matrix raw materials, which formed a TiC particle layer between the carbon rich layer and the matrix, and resulted in a greater coherent bonding between these two interfacial layers [44]. The TiO_2 dopant introduction (LAS IV) contributed to the decrease in flexural strength of the composite to less than 500 MPa. This implies that titania additions chemically attack the fibre, depleting its strength, perhaps due to formation of surface defects.

4. Conclusion

Nicalon SiC fibre uniaxially reinforced $Li_2O \cdot Al_2O_3 \cdot 6SiO_2$ glass–ceramic composites were fabricated and demonstrated high flexural strength (>800 MPa) and fracture toughness, K_{IC} (>15 MPa $m^{1/2}$). Ta_5O_5 and Nb_2O_5 acted as effective nucleating agents in the glass matrices and also formed interfacial carbide (TaC and NbC) layers between the fibre and the matrix, which improved the mechanical properties of the composites. The amorphous carbon rich layer and the carbide layer in the interfacial region resulted in low interfacial shear strength between the fibre, matrix and the permitted fibre pull-out, which led to high toughness in the composites. The composite with TiO_2 additive in the matrix showed a lower flexural strength (<500 MPa) and smaller K_{IC} value (<11 MPa $m^{1/2}$) which resulted from high interfacial shear strength between the SiC fibres and the matrix due to the formation of a TiC layer in this interfacial region.

References

1. D. BELITSKUS, *Materials & Design* **10** (1989) 2.
2. K. K. CHAWLA, in "Composite material, science and engineering" (Springer-Verlag, New York, 1987) p. 135.
3. J. J. MECHOLSKY, *Amer. Ceram. Bull.* **68** (1988) 367.
4. D. R. JOHNSON, A. C. SCHAFFHAUSER, V. J. TENNERY, E. L. LONG Jr. and R. B. SCHULZ, *Amer. Ceram. Soc. Bull.* **64** (1985) 276.
5. K. M. PREWO, J. J. BRENNAN and G. K. LAYDEN, *ibid.* **65** (1986) 305.
6. S.-T. BULJAN, A. E. PASTO and H. J. KIM, *ibid.* **68** (1989) 387.
7. K. M. PREWO, *ibid.* **68** (1989) 395.
8. *Idem., J. Mater. Sci.* **21** (1986) 3590.
9. P. G. CHARLAMBIDES and A. G. EVANS, *J. Amer. Ceram. Soc.* **72** (1989) 746.
10. M. D. THOULESS, O. SBAIZERO, L. S. SIGL and A. G. EVANS, *ibid.* **72** (1989) 525.
11. A. G. EVANS and M. Y. HE, *ibid.* **72** (1989) 2300.
12. R. W. RICE, *Ceram. Engng Sci. Proc.* **2** (1978) 694.
13. V. V. KRISTIE and P. S. NICHOLSON, *J. Amer. Ceram. Soc.* **64** (1981) 499.
14. A. G. EVANS, *Philos. Mag.* **26** (1972) 1372.
15. L. L. LANGE, *ibid.* **22** (1980) 983.
16. J. J. BRENNAN and K. M. PREWO, *J. Mater. Sci.* **17** (1982) 2371.

17. K. M. PREWO, in Proceedings of the 21st University Conference on Ceramic Science, Penn. State Univ. (Plenum, New York) July, 1985.
18. R. W. RICE, *Ceram. Engng Sci. Proc.* **5** (1985) 589.
19. F. K. KO, *Amer. Ceram. Soc. Bull.* **72** (1989) 401.
20. R. A. SAMBELL, D. H. BOWEN and D. C. PHILIPS, *J. Mater. Sci.* **7** (1972) 663.
21. R. A. SAMBELL, D. H. BOWEN and D. C. PHILIPS, *ibid.* **7** (1972) 676.
22. D. C. PHILIPS, R. A. SAMBELL and D. H. BOWEN, *ibid.* **7** (1972) 1454.
23. D. C. PHILIPS, *ibid.* **9** (1974) 1847.
24. S. R. LEVITT, *ibid.* **8** (1973) 793.
25. J. BACON, K. M. PREWO and R. VELTRI, in Proceedings of the 1978 International Conference on Composite Materials, Töronto, Canada, AIME (1978) p. 753.
26. E. R. THOMPSON and K. M. PREWO, in Proceedings of the 21st Structures, Structural Dynamics & Materials Conference (1980) p. 539.
27. S. YAJIMA, K. OKAMURA, J. HAYASHI and M. OMORI, *J. Amer. Ceram. Soc.* **59** (1976) 324.
28. T. MAH, N. L. HECHT, D. E. McCULLUM, J. R. HOENIGMAN, H. M. KIM, A. P. KATZ and H. A. LIPSITT, *J. Mater. Sci.* **19** (1984) 1191.
29. T. J. CLARK, M. JAFFE, J. RABE and N. R. LANGLEY, *Ceram. Engng. & Sci. Proc.* **7** (1986) 901.
30. L. C. SAWYER, R. T. CHEN, F. HAIMBACH, P. J. HARGET, E. R. PRACK and M. JAFFE, *ibid.* **7** (1986) 914.
31. K. L. LUTHERA, *J. Amer. Ceram. Soc.* **69** (1986) C231.
32. K. M. PREWO and J. J. BRENNAN, *J. Mater. Sci.* **15** (1980) 463.
33. K. M. PREWO and J. J. BRENNAN, *ibid.* **17** (1982) 1201.
34. M. A. HERRON and S. H. RISBUD, *Amer. Ceram. Soc. Bull.* **65** (1986) 342.
35. D. P. STINTON, A. J. CAPUTO and R. A. LOWDEN, *Amer. Ceram. Soc. Bull.* **65** (1986) 347.
36. A. J. ECKEL and R. C. BRADT, *J. Amer. Ceram. Soc.* **72** (1989) 455.
37. J. J. BRENNAN, in Proceedings of the 21st University Conference on Ceramic Science, Penn. State Univ., (Plenum, New York) July, 1985. p. 549.
38. R. CHAIM and A. H. HEUER, *Advan. Ceram. Mater.* **2** (1987) 154.
39. E. BISCHOFF, M. RÜHLE, O. SBAIZERO and A. G. EVANS, *J. Amer. Ceram. Soc.* **72** (1989) 741.
40. R. F. COOPER and K. CHYUNG, *ibid.* (1987) 3148.
41. K. M. PREWO, *J. Mater. Sci.* **22** (1987) 2695.
42. J. Y. HSU and R. F. SPEYER, *J. Amer. Ceram. Soc.* **72** (1989) 2334.
43. J. Y. HSU and R. F. SPEYER, *J. Am. Ceram. Soc.* **74** (1991) 395.
44. J. Y. HSU and R. F. SPEYER, "Interfacial Phenomenology of SiC Fiber Reinforced $Li_2O \cdot Al_2O_3 \cdot 6SiO_2$ Glass-Ceramic Composite", Submitted to J. Mater. Sci.
45. ASTM Standard Test Method, E 399-83.
46. S. T. ROLFE and J. M. BARSOM, in "Fracture and fatigue control in structures" (Prentice-Hall, Inc., Englewood Cliffs, 1977) p. 52.
47. D. B. MARSHALL, *J. Amer. Ceram. Soc.* **67** (1984) 259.
48. D. B. MARSHALL, *J. Amer. Ceram. Soc.* **68** (1985) 225.
49. T. W. COYLE, H. M. CHAN and U. V. DESHMUKH, in "Effects of heat treatments in air on the microstructure and mechanical behaviour of the fiber/matrix interface in an LAS glass-ceramic matrix-SiC fiber composite", edited by H. Ishida (Elsevier, NY, 1988) p. 489.
50. P. W. McMILLAN, "Glass Ceramics" in "Non-metallic solids: a series of monographs", edited by J. B. Roberts and P. Popper, Vol. 1, 2nd Edition (Academic Press, London, 1979) p. 165.

Received 2 July 1990
and accepted January 1991